

DEPARTMENT OF MECHANICAL ENGINEERING  
ME4-CFD INDIVIDUAL PROJECT

---

---

**CFD Analysis of the flow around an  
aircraft**  
**Technical Report**

---

---

Author:  
Theophile SAUTORY  
Word count: 3,935

March 14<sup>th</sup>, 2019, South Kensington

# Abstract

The role of this report was to fully explore the CFD analysis of the flow around an aircraft using three different turbulence models: Standard  $k - \epsilon$ , SST  $k - \omega$ , and the Quadratic Pressure Strain Reynolds Stress model with high  $y_w^+$  wall treatment. The mesh generation is extensively described, through the aircraft positioning, creation of volumetric controls, specific surface region meshes and prism layer thickness to ensure a  $y_w^+$  in the range [30, 200]. The grid refinement study on the most demanding set-up (namely RST model at maximum velocity) revealed that integral quantities varied by less than 0.03% in meshes above 1.97 million cells. The 1.97 million cells mesh was selected for the rest of the analysis. An iterative procedure was ran to compute the minimal take off speed of the aircraft, resulting in values 2.1 times higher than those expected from literature. Potential factors for this discrepancy are the geometry of the plane which should vary at take off, and the assumption of constant weight during take off. The AOA analysis resulted in similar general trends for the three turbulent models, whilst their comparison with literature validated the simulations. The lift coefficient was seen to increase up to an angle in the range of  $5 - 10^\circ$ , while the drag was seen to increase quadratically with the angle of attack. Additional vector plots of the line integral convolution of velocity enabled to explore the flow physics behind these graphs. The plots form the  $k - \omega$  model revealed that above an AOA of  $5^\circ$ , flow separation occurred, reversing the flow and driving a decrease in lift coefficient and drastic increase in drag coefficient. Finally, the pressure coefficient was plotted around the wing to compare the general trend with airfoils from literature. The plot highlights erroneous trends near the flaps, potentially revealing a mesh design flaw. Overall, this CFD analysis seems to provide plausible results from the engineering point of view, and allowed to explore the flow aerodynamics around an aircraft as well as the CFD computational method.

# Contents

<b>1</b>	<b>Introduction and Objectives</b>	<b>1</b>
1.1	Introduction . . . . .	1
1.2	Objectives . . . . .	2
<b>2</b>	<b>Methodology</b>	<b>3</b>
2.1	Dimensional and Non-Dimensional Study . . . . .	3
2.1.1	Dimensional Study . . . . .	3
2.1.2	Non-Dimensional Parameters Study . . . . .	3
2.1.3	Flow Physics . . . . .	4
2.2	Simulation Set-up . . . . .	5
2.2.1	Positioning the aircraft in the Wind-Tunnel . . . . .	5
2.2.2	Creating a single region . . . . .	6
2.2.3	Flow around the aircraft . . . . .	6
2.2.4	Aircraft Surface . . . . .	6
2.2.5	Near wall consideration . . . . .	7
2.2.6	Summary values . . . . .	8
2.2.7	The three turbulence models analysed . . . . .	8
2.2.8	Boundary Conditions . . . . .	8
<b>3</b>	<b>Results and Discussion</b>	<b>9</b>
3.1	Grid Refinement Study . . . . .	9
3.1.1	Set-Up . . . . .	9
3.1.2	Results and Discussion . . . . .	9
3.2	Minimum Take-off Speed . . . . .	10
3.2.1	Set-Up . . . . .	10
3.2.2	Results and Discussion . . . . .	11
3.3	Angle of Attack Analysis . . . . .	11
3.3.1	Set-Up . . . . .	11
3.3.2	Results and Discussion . . . . .	12
3.4	Comparison With literature . . . . .	15
3.4.1	Set-Up . . . . .	15
3.4.2	Results and Discussion . . . . .	15
<b>4</b>	<b>Conclusions</b>	<b>17</b>
<b>5</b>	<b>References</b>	<b>18</b>

# 1 Introduction and Objectives

## 1.1 Introduction

Computational Fluid Dynamics (CFD) is a field focused on replacing the partial differential equations which govern fluid flows in sets of algebraic equations, to then solve them with digital computers and numerical methods. Over recent years, CFD emerged as a suitable solution to reduce the use of wind tunnel experiments, consequently reducing the cost of engineering products development [1]. The importance of understanding fluid flows emerges in many engineering applications, ranging from oil industry to weather forecasting passing through aircraft design process. The role of this report is to perform a CFD analysis using the STAR-CCM+ software, over the Hercules C-130J aircraft, investigating various turbulence models and analysing the simulations' results to comment on their accuracy and plausibility. The plane of interest is shown in figure (1.1), even though the studied model does not have the back wing.



**Figure 1.1:** Hercules C-130 J aircraft [2]

Using CFD on an aircraft is essential to understand the flight control and stability in different flow regions. In the present analysis, a CFD study is performed to explore the dependency of integral flow quantities on grid refinement, to develop a suitable way to resolve the flow whilst limiting the use of computer power. The mesh should respect the aircraft complex geometry to ensure the quality of the results in the plane critical areas. Moreover, multiple physics models are investigated to observe the differences in results in lift in drag coefficients with given angles of attack, and in estimating the flight minimum take-off speed.

## 1.2 Objectives

The main objectives of this analysis are threefold:

- **Confirm that integral quantities of relevance become grid independent once the mesh becomes finer**, by investigating four different meshes with varying refinement levels on the most demanding turbulence model set-up of interest.
- **Determine and discuss the minimal take-off speed obtained using the three different turbulence models of interest.**
- **Investigate, compare, and critically analyse the impact of the angle of attack on integral quantities for each turbulence model at cruising speed**, revealing both qualitative and quantitative results.

# 2 Methodology

The first step of the CFD analysis was to create the simulation set-up and a well refined mesh for the plane wind-tunnel domain. The generated mesh must both ensure it captures the whole flow dynamics and geometric features, as well as ensuring the simulation is not too computationally costly, implying that the mesh used throughout the analysis should not exceed 2 million cells [3]. To start off, a dimensional and non dimensional analysis of the tackled problem must be held.

## 2.1 Dimensional and Non-Dimensional Study

### 2.1.1 Dimensional Study

The use of a CFD analysis, comprising of the modelling of a plane in a wind-tunnel allows to circumvent the problem of scaling the aircraft. Indeed, the plane, imported as a .stl file for the project, was set to its actual length, in order to directly match the results to the real size model. The key dimensions of the Hercules C-130J aircraft are described in table 2.1 [4].

**Table 2.1:** C-130 Hercules Carrier Characteristics

Hercules C-130 Characteristics	Value	Unit
Length	29.79	m
Height	11.61	m
Total Wing Area	162.1	m
Empty Weight	37,648	kg
max. Takeoff Weight	70,307	kg
empty. Takeoff Weight	37,648	kg
Cruise Velocity	179	$\text{m.s}^{-1}$
Maximum Velocity	186	$\text{m.s}^{-1}$
Cruise Altitude	6076	m

### 2.1.2 Non-Dimensional Parameters Study

Flight aerodynamics can be defined by key dimensionless quantities. The latter allow to learn about the flow physics taking place in the set-up, and enable to compare two similar experiments of different scales. As these numbers translate the flow physics, they play a crucial role in the definition of the physics models which have to be used, and the assumptions which can be made. In the scope of this project, the first non-dimensional number of interest is the Reynold's number, given by (2.1):

$$Re = \frac{\rho U_\infty L}{\mu} \quad (2.1)$$

The Reynold's number corresponds to the ratio of the inertial forces to the viscous forces, where  $\rho$  and  $\mu$  are the density (in  $\text{kg.m}^{-3}$ ) and dynamic viscosity (in  $\text{Ns.m}^{-2}$ ) of a fluid respectively, while  $L$  is the characteristic length of the flow geometry in (m), of stream velocity  $U_\infty$  in ( $\text{m.s}^{-1}$ ). Over a flat plate, the transition between laminar and turbulent flow regimes occurs at  $Re \approx 5 \times 10^5$  [5]. Hence, this number is of extreme importance and is computed in table 2.2, revealing the turbulent nature of the flow, paving the way for the turbulence models to be used to resolve it. Moreover, as a ratio of forces, a similarity in  $Re$  implies a similarity in the forces' ratio, whatever the model used to resolve the flow dynamics.

A flow is also defined by a velocity, and its non-dimensional definition: the Mach number. The latter is the ratio of the flight velocity  $U$  to the local speed of sound  $a$ , both in  $\text{m.s}^{-1}$  (2.2):

$$Ma = \frac{U}{a} \quad (2.2)$$

This non-dimensional parameter is essential as it describes the compressible effects taking place in the flow. Above a Mach number of 0.2-0.3, the incompressibility assumption is invalid [6]. Hence, from the values exposed in table 2.2, the ideal gas law was used instead of the constant density assumption.

Finally, the force components of lift and drag also define the flow of interest with non-dimensional numbers. Indeed, the lift  $C_L$  and drag coefficients  $C_D$  (2.3), are non dimensional expressions related to these forces, and enable the comparison of the the different simulations and different scaled experiments. They serve as validation parameters to compare between the different models used and with reference values taken from literature.

$$\begin{cases} C_L = \frac{Li}{\frac{1}{2}\rho U_\infty^2 S} \\ C_D = \frac{D}{\frac{1}{2}\rho U_\infty^2 S} \end{cases} \quad (2.3)$$

where  $S$  is the characteristic area of the element on which the force act in  $\text{m}^2$  and  $Li$  and  $D$  are the lift and drag forces respectively, in  $N$ .

### 2.1.3 Flow Physics

The flow physics properties at cruise altitude for the simulations are summarised in table 2.2. Revealing both turbulence and compressibility.

**Table 2.2:** Flow Physics Properties at Cruise Altitude

Property	Nomenclature	Value	Unit
Altitude	$h$	6076	m
Free-stream Temperature	$T$	248	K
Free-stream Density	$\rho$	0.49	$\text{kg.m}^{-3}$
Free-stream Velocity	$U_\infty$	172	$\text{m.s}^{-1}$
Length Scale	$L$	3.9	m
Dynamic Viscosity	$\mu$	1.58E-5	$\text{Ns.m}^{-2}$
Cruise $Re$	$Re_c$	2.08E+7	-
Max Velocity $Re$	$Re_m$	2.25E+7	-
Speed of Sound	$a$	316.0	$\text{m.s}^{-1}$
Mach at Cruise	$Ma_c$	0.54	-
Mach at MaxVel	$Ma_m$	0.59	-

## 2.2 Simulation Set-up

After having selected the critical dimensionless numbers describing the flow, the CFD region and mesh were generated to resolve the flow of the problem.

### 2.2.1 Positioning the aircraft in the Wind-Tunnel

The wind-tunnel and aircraft were imported as .stl files, and were given in the scope of the project. To capture the essential characteristics of the flow, it was necessary to position the aircraft in a adequate position in the wind-tunnel box. As the most important flow characteristics are expected to be in the wake of the plane, a length of two planes was left behind the actual plane as shown in the z axis of figure 2.1, to capture the whole flow dynamics. To allow for the flow to develop before encountering the plane, a length of one plane was left at the entry. As the plane is symmetrical with respect to its centre plane, the analysis was only held on half of the plane. This enables to divide the number of cells by two when compared to a whole plane analysis, allowing for a finer mesh. Hence, the mid plane section of the aircraft was set to be in contact with the  $x = 0$  boundary of the wind-tunnel surface. Finally, the aircraft was set to the middle height (y axis) of the wind-tunnel, to capture the flow around the top and bottom surfaces of the plane. This generic set-up was held for both the grid refinement study at maximum speed, and the angle of attack analysis.

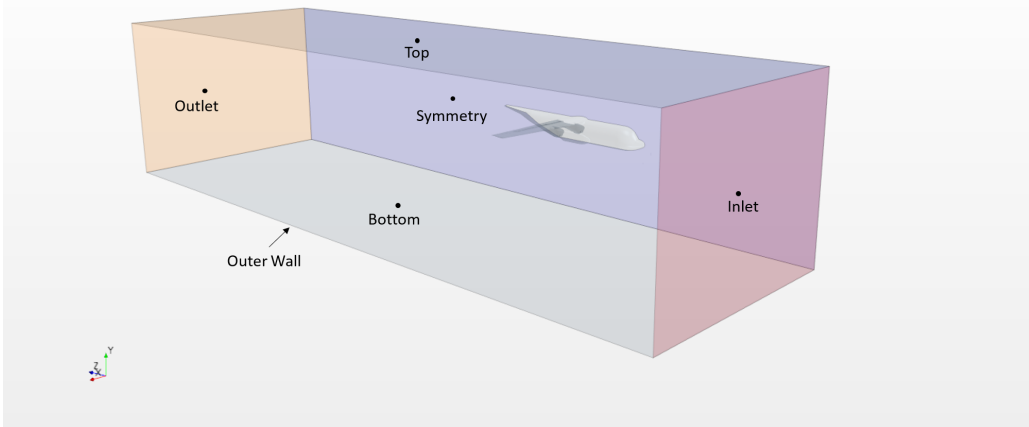


**Figure 2.1:** Plane set-up in the wind-tunnel

## 2.2.2 Creating a single region

To create a single region from the aircraft and wind-tunnel to run the simulations, the boolean 'subtract' function was used. Splitting the wind-tunnel surfaces by angle gave rise to seven respective surfaces (counting the subtract) as showed in figure 2.1. This allowed to set the respective boundary conditions, described in the boundary conditions section 2.2.8 of the report.

## 2.2.3 Flow around the aircraft

As the wind-tunnel captures an exhaustive flow region around the aircraft, smaller volumetric controls were constructed around the aircraft with smaller cell sizes around the engines, fuselage, wing and wake, to compute the flows details more accurately. These are summarized in table ??

**Table 2.3:** Volumetric Controls

Volumetric Controls	Custom Trimmer Size (% of base)
Whole Aircraft	20
Engines & Wing	10
Flaps & Flaps Wake	3

## 2.2.4 Aircraft Surface

The aircraft model on which the analysis is held is a very complex geometry due to the different curves and shapes which form it. Hence, it must be treated with care to ensure that the mesh keeps the correct geometric shape. Star-CCM+ offers the surface wrapper and remesher functions to preserve such a geometry. The latter are used in conjunction to prevent 'leakage' in the mesh, and prevent gaps in the plane's geometry to the fluid domain which could introduce geometry distortion effects [7]. After having completed some preliminary meshes of the aircraft, it also appeared clearly

that certain regions required additional care to reach a high cell quality. Thus, the aircraft was split by surfaces manually, being able to mesh specific regions with higher number of cells, to ensure that the geometry and edges were respected. The different surface meshes are detailed in table 2.4.

**Table 2.4:** Aircraft Surface Mesh

Surface	Custom Surface Size (%base)	
	Target	Minimum
Main Body & Exterior Flap	5	2.5
Interior Flap	2	1
Engines Front & Connection between Wing and Main Body	1.5	1

This resulted in a high cell quality at the surface, as shown in figure 2.2.

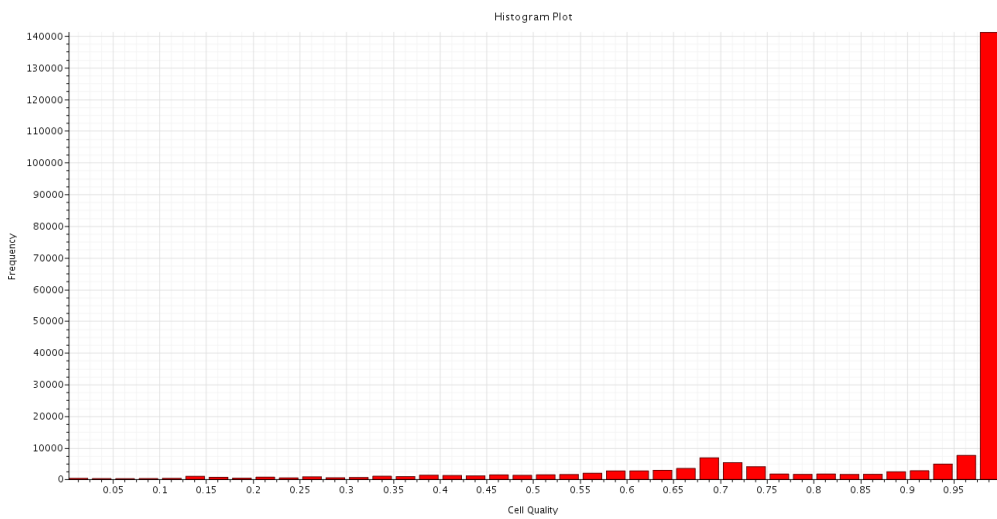


**Figure 2.2:** Histogram of cell quality

Finally, the contact prevention function was used between the flaps as is it an essential region for flow dynamics. This was done to conserve the initial geometry and prevent a broken down geometry (or the creation of a contact surface in between the flaps) from negatively impacting the computed solution.

## 2.2.5 Near wall consideration

In the scope of our project analysis, any wall integrated approach could not be used because of the additional computational power they required [3]. Hence, the mesh quality had to be in accordance with the use of wall functions. The latter does not affect the bulk turbulence model, but only the near wall region. As the boundary layer -which represents the most complex dynamic region of the turbulent flow- develops at the wall, the first prism cell should not discretise the largest gradients occurring at the wall itself as there is no wall integrated approach. Hence the wall  $y_w^+$  should be in the following range:  $30 < y_w^+ < 200$  [3]. This was a crucial parameter in our model set-up.

## 2.2.6 Summary values

A solution for the mesh design for the aircraft was the use of trimmer cells (octree), especially as it allows for an easy control of volumetric refinement [3]. However, the first cell must remain very close to the wall to efficiently capture the layer, whilst it can extend in directions parallel to the wall. Hence, prism layers were used in conjunction of the octree cell. The absolute value of the prism layer thickness was set to 0.1 m as revealed in 2.5, to ensure  $y_w^+$  remained in the defined range.

**Table 2.5:** Surface Prism Layers

Number of Prism Layers	Prism Layer Stretching (% of base)	Absolute Prism Layer Thickness (m)
8	1.5	0.1

## 2.2.7 The three turbulence models analysed

The analysis consisting of comparing different turbulence models was held on the following three models, which can be compared on how they can be used with the wall function used in the generated mesh [7].

- Standard  $k - \epsilon$  two-layer all  $y_w^+$ : by having a two layer approach, two dissipation rates  $\epsilon$  and turbulent viscosity  $\mu_t$  are computed close and far from the wall. Hence, the model is described as being compatible with wall functions as long as  $y_w^+ > 30$ .
- SST  $k - \omega$ : by blending a  $k - \epsilon$  layer in the far stream to a  $k - \omega$  layer near the wall following [8] approach, the model is compatible with the wall function approach with  $y_w^+ > 30$ .
- Quadratic Pressure Strain Reynolds Stress model with high  $y_w^+$  wall treatment (RST): by its definition of high  $y_w^+$  wall treatment, the model is compatible with the wall function treatment.

## 2.2.8 Boundary Conditions

After having created an adequate mesh for the simulations and chosen the different models to test, the flow boundary conditions were set and summarised in table 2.6, and the analysis could be started.

**Table 2.6:** CFD simulation analysis Boundary Conditions

Boundary	Boundary Conditions
Aircraft Surface	No-slip wall
Top	Slip wall
Bottom	Slip wall
Inlet	Inlet Velocity
Outlet	Pressure Outlet
Symmetry	Symmetry Plane
Outer Wall	Slip wall

# 3 Results and Discussion

The following section describes the set-up, results, and discussion of the analysis of the flow around an aircraft. The grid refinement study is explained, before looking at the minimal take-off speed for the three different turbulence models, the influence of angle of attack on integral quantities, and how our analysis can compare to literature.

## 3.1 Grid Refinement Study

### 3.1.1 Set-Up

The first step of the analysis was to investigate the evolution of integral quantities with respect to the refinement level. This is essential to ensure that the studied mesh is fine enough to satisfy the discretisation error requirement [3]. Hence, the refinement study was held by varying the reference grid size, and running for the most demanding simulation: RST model at plane maximum velocity [3]. Table 3.1 reveals the different values on which the analysis was held.

**Table 3.1:** Refinement Study Meshes

Refinement	Base Size (m)	No of cells (millions)
Very Coarse	2.5	0.801
Coarse	1.8	1.31
Reference	1.6	1.97
Fine	1.5	2.94

### 3.1.2 Results and Discussion

The integral quantities computed ( $C_l$  and  $C_d$ ) were plotted against the grid size in figure 3.1. This plot highlights the impact of mesh refinement on flight parameters. Indeed, it can be seen that the lift coefficient seems to be constant for grid refinements above 1.97 million cells. A similar analysis is held for the drag coefficient, with the value converging for the highest size meshes. Therefore, this analysis successfully reveals that integral quantities of relevance become grid independent at high levels of refinement. This serves to reinforce the idea that holding the rest of the analysis on a mesh of 1.97 million is sensible, as the computational time is greatly reduced when compared to the 2.94 million cells mesh, whilst the results are steady, varying by less than 0.03%. On the other

hand, the coarse meshes failed to converge to the apparently correct value due to its comparatively large cells, which make it unable to accurately resolve the aircraft geometry properly.

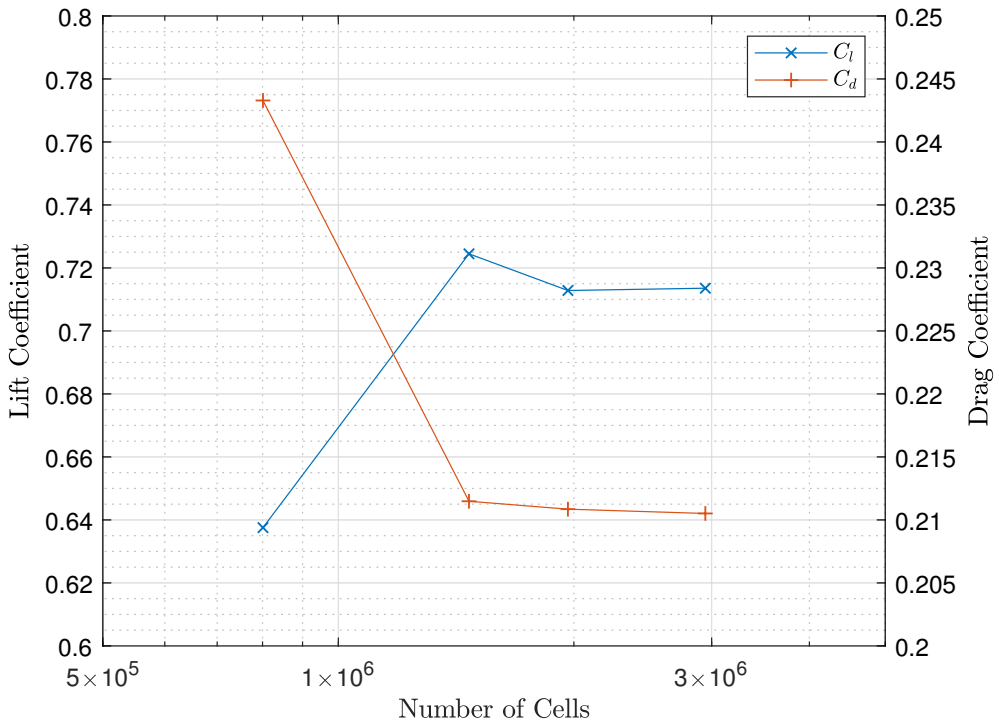


**Figure 3.1:** Histogram of cell quality

## 3.2 Minimum Take-off Speed

The second set of results which were to be computed for the aircraft analysis were the minimal take-off speed for each of the three turbulence models of interest.

### 3.2.1 Set-Up

To perform this analysis, the plane was now set at the bottom of the wind-tunnel, directly in contact with the floor to mimic take-off, whilst the floor boundary condition was switched to a no-slip condition with a tangential velocity equal to that of the inlet, as it did not represent the free-stream anymore. The plane was set parallel to the floor, assuming the angle of attack during take-off to be 0. Moreover, as the .stl part is fixed, the plane geometry was assumed to be exactly the same at take-off than during cruise, implying that the flaps are not rotated. Finally, the mass of the plane was taken as constant during take-off for simplicity, hence neglecting the mass of fuel lost before the actual take-off. The pressure was then assumed to be 1 atm, whilst the density  $\rho$  was set to  $1.225 \text{ kg.m}^{-3}$  and the temperature  $T$  to 288 K; corresponding to standard atmospheric conditions.

As the aircraft is desired to take off, the equation for lift can be rewritten giving (3.1) [9], with  $W$  being the minimal take off weight from table 2.1 as we are searching for the minimal take-off speed:

$$U_{stall} = \sqrt{\frac{W}{\frac{1}{2}\rho C_{lmax} S}} \quad (3.1)$$

The take-off velocity is expressed as (3.2) [9]:

$$U_{take\ off} = 1.2U_{stall} \quad (3.2)$$

To find the correct value of  $U_{take\ off}$ , an iterative procedure was used. Indeed, an initial value of 90 m.s<sup>-1</sup> [10] was used to run a first simulation. A corresponding  $C_l$  was then computed by running the simulation. This then allowed to calculate a value for  $U_{take\ off}$  using (3.1) and (3.2). Iterations were made until the computed value of  $U_{take\ off}$  was found to match to + or - 1 m.s<sup>-1</sup> of the previous guess. Table 3.2 shows the obtained results.

### 3.2.2 Results and Discussion

**Table 3.2:** Minimal take-off speed

Model	$C_l$	$U_{take\ off}$ m.s <sup>-1</sup>
$k - \epsilon$	0.91	75.9
$k - \omega$	0.89	76.7
RST	0.85	78.6

The computed velocities are higher than the values mentioned in literature for the Hercules C-130J aircraft of 36.2 m.s<sup>-1</sup> [4]. The first reason for such a discrepancy could rely on the low computed  $C_l$  value. Indeed, during take-off, extra flaps might be deployed, further increasing lift and decreasing the velocity. Moreover, the absence of the tail on the wing plays a role in affecting the geometry and hence the lift coefficient value. Finally, the overall quality of the mesh can also be mentioned as a potential factor affecting the plane take off speed. The three different values are observed for the different turbulence models due to the different values they provide for the lift coefficient, revealing preliminary differences in their solutions.

## 3.3 Angle of Attack Analysis

Analysing the flow dynamics with given angles of attack (AOA) is of drastic importance in aerodynamic flows. Indeed, it serves to explain wind stalling and the overall angle capability of the airplane.

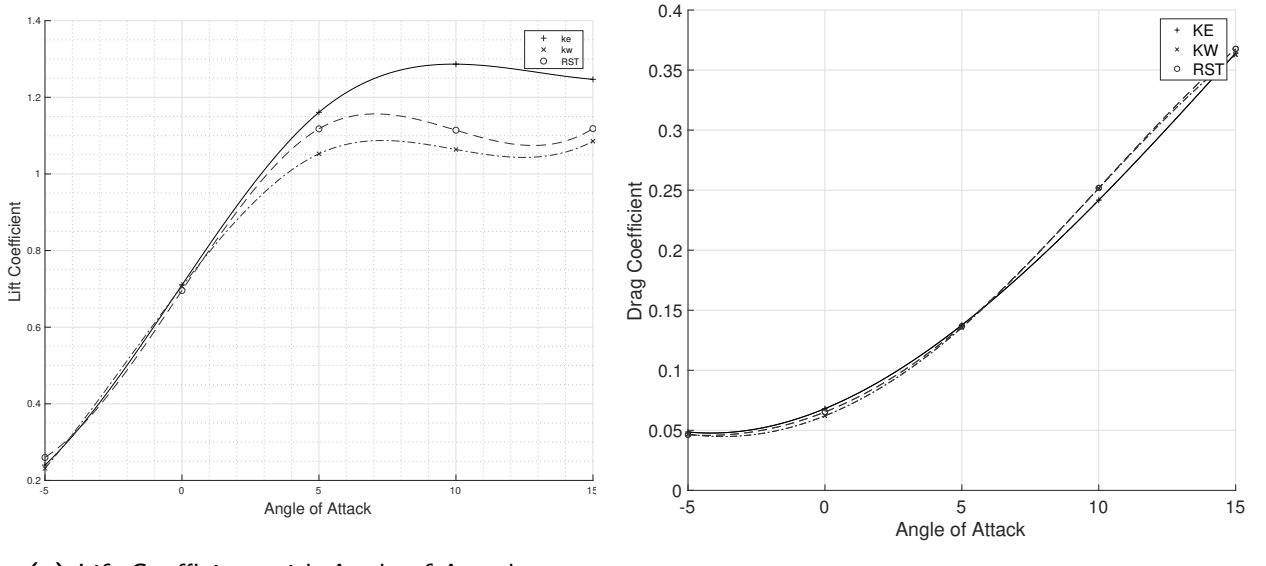
### 3.3.1 Set-Up

To analyse the variation in integral values with AOA for the three turbulence models, the plane was rotated in a range of [-5° ; 15°], with a rotation step of 5°. The respective boundary conditions

on the wind-tunnel were left untouched from section 2.2.8 as the simulation set-up itself was not varied. Moreover, it was set back to the generic position described in section 2.2

### 3.3.2 Results and Discussion

The results of the experimentation are revealed in figures 3.2a and 3.2b, where the dots are connected by expected splines. It appears that the results for the lift coefficient for each of the turbulent model showed in figure 3.2a follow the same trend up to  $\approx 8^\circ$ , having a steady and nearly linear increase from  $-5^\circ$  to a maximum ranging between  $5^\circ$  and  $10^\circ$ . The point where the lift coefficient starts to fall is referred to as stall [10]. Up to this point, the result actually follow the expected trends from literature [10]. However, the fact that the results both show an increase after  $10^\circ$  for the  $k - \omega$  and RST model separates from literature plots. This observation might be due to errors in the mesh or convergence issues. It is also noted that the  $k - \epsilon$  model seems to evaluate at a higher value the lift coefficient than the RST model, which in terms evaluates at a higher value than the  $k - \omega$  model. This is due to the differences in the way they model the turbulent energy and viscosity.



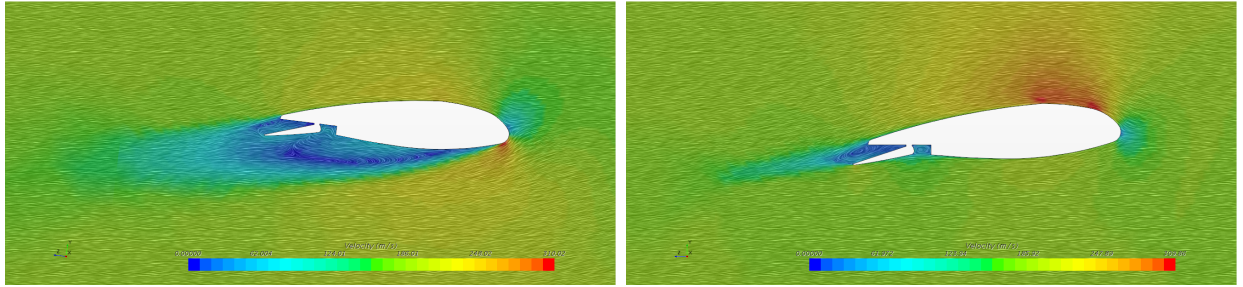
(a) Lift Coefficient with Angle of Attack

(b) Lift Coefficient with Angle of Attack

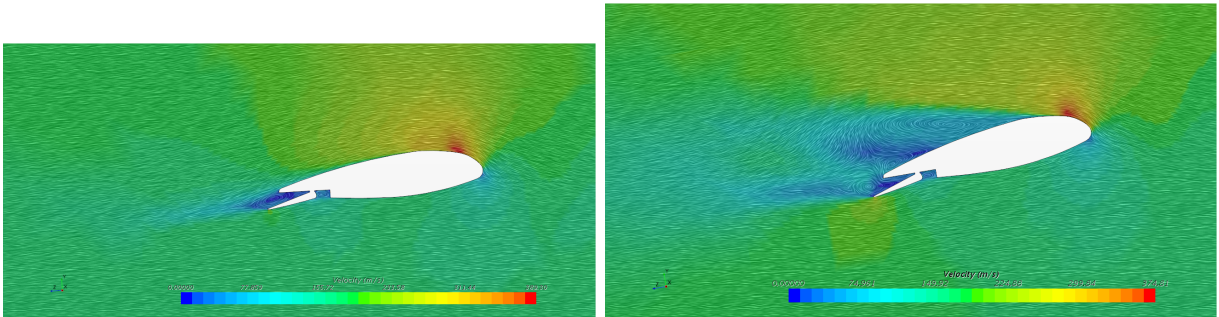
**Figure 3.2:** Lift (a) and Drag (b) Coefficients as a function of the Angle of Attack

On the other hand, the results for the drag coefficient seem to be in line with literature [10] and to coincide between each model. The drag coefficient is seen to increase quadratically with the AOA, without having a change in slope as for the lift coefficient.

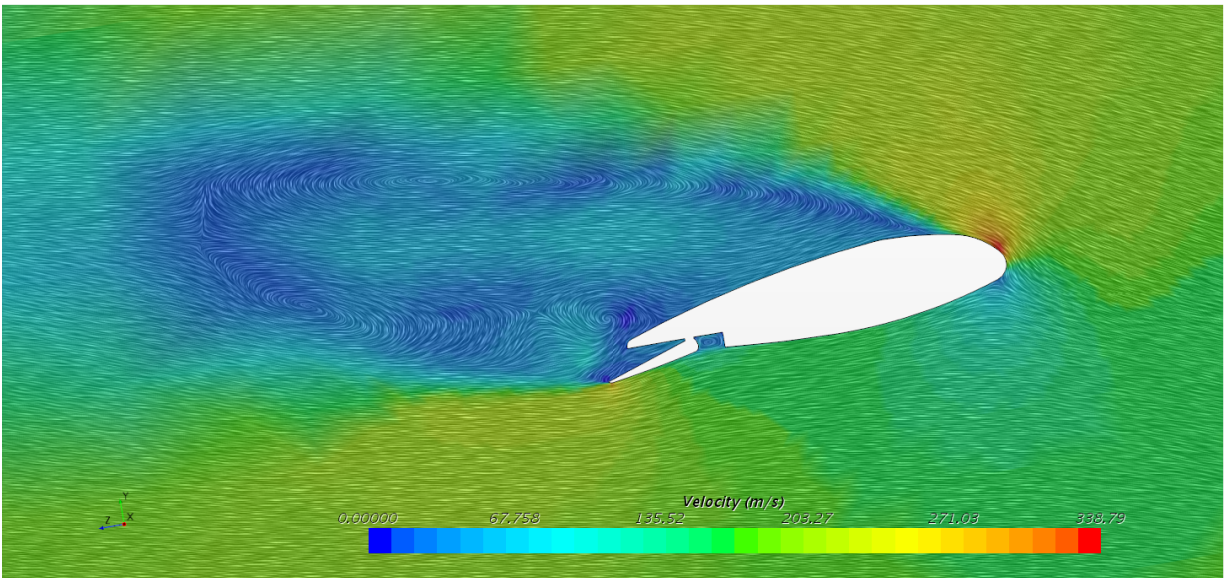
To understand the flow physics behind the observed trends in figure 3.2, line integral convolutions of the velocity field were plotted at different flow angles for the  $k - \omega$  model. These enable to visualize the fluid motion around a section of the airfoil in between the two engines.



(a) -5° angle of attack, velocity scale: 0 to 309 (b) 0° angle of attack, velocity scale: 0 to 310  
m.s<sup>-1</sup>



(c) 5° angle of attack, velocity scale: 0 to 389 (d) 10° angle of attack, velocity scale: 0 to 374  
m.s<sup>-1</sup>



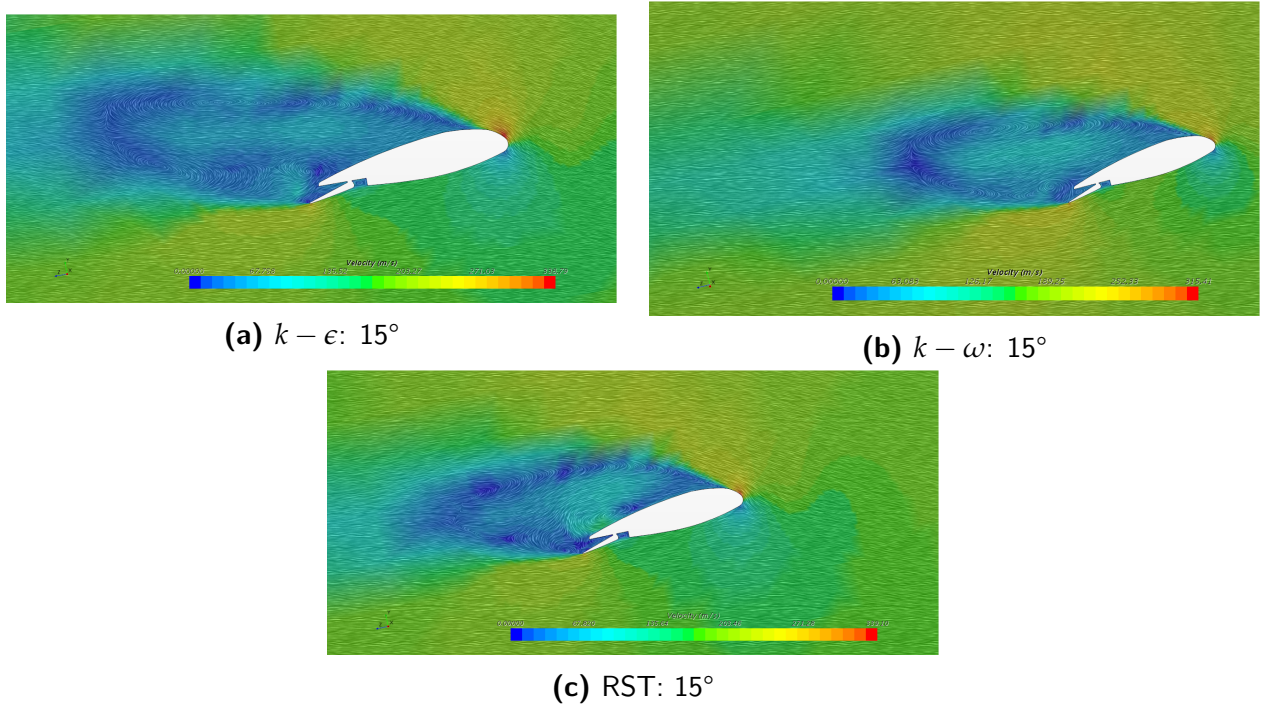
(e) 15° angle of attack, velocity scale: 0 to 338 m.s<sup>-1</sup>

**Figure 3.3:** Vector plots of  $k-\epsilon$  simulations for varying angle of attacks

As the AOA increases, the velocity scale does too. This translates the idea that the average velocity over the top of the wing increases from -5° to 5°. In terms, this induces a region of low pressure above the wing surface as the kinetic energy increases, which will act as suction. Therefore, the force due to pressure difference between the top and bottom region of the surface will increase, driving a similar increase in lift coefficient. This explains the positive slope from the lift coefficient with increasing AOA until 5°. However, it is seen that for 10°, the flow separates on the top of the airfoil (figure 3.3d). This is due to the large adverse pressure gradients acting on the smooth surface [11]. This, in terms creates a shear boundary layer, and figure 3.3d reveals that the flow does not reattach

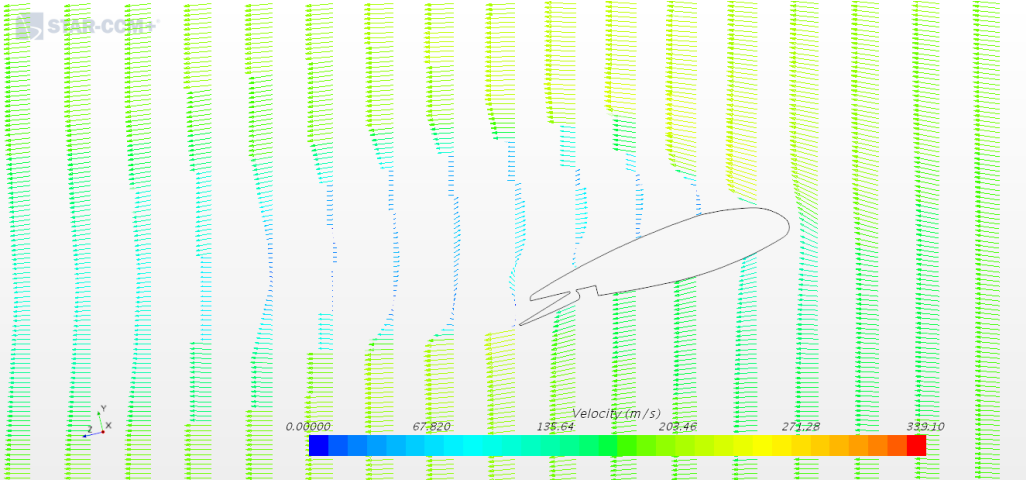
at the end of the wing. This corresponds to the observation of stall. The separation is even more apparent for figure 3.3e, where the large recirculation of the flow takes place on the entire top surface of the wing. These observations explain the significant increase in drag from figure 3.2b. Indeed, as the recirculation zone becomes greater, there is a greater region of low pressure in the wake of the airfoil. Hence, the force due to pressure difference at the front and back of the airfoil balloons, driving the pressure drag. Moreover, as the angle increases, the frontal area increases due to rotation. Therefore, the drag force shoots up too. From this extended analysis, the results seem to make sense in an engineering point of view, validating in a way the general trends observed from the held CFD analysis. The trends for the other turbulence models are similar, and are therefore not exhibited.

Figure 3.4 shows the plots for the three different models at  $15^\circ$ , where flow separation occurs. The three flows reveal similar trends reflecting the flow detachment causing the large drag values.



**Figure 3.4:** Qualitative results of the angle of attack study showing vector plots for the  $k - \omega$ ,  $k - \epsilon$  and RST models at  $15^\circ$

To explore the reason for flow separation, the streamlines for the RST model rotated at  $15^\circ$  were plotted in figure 3.5. In this set-up, flow separation occurred, as shown in figure 3.4c. The streamlines highlight the idea of pressure gradients opposing the flow direction. Indeed, the boundary layer starts to develop at first but then reverses. A shear layer prevents its development and the negative pressure gradient is such that the flow is reversed. This explains the large recirculation region and the resulting increase in drag coefficient.



**Figure 3.5:** Streamlines Plot at 15 °RST

Therefore, the principal observations made from our CFD analysis on the impact of AOA on the flow solution seem to be reasonable and plausible from an engineering point of view. However, the trend for the lift coefficient is seen to separate from literature values. A potential way to improve the observations would have been to run the simulations at even higher angles, and potentially smaller step size between the angles to prevent from interpolating as much as on figure 3.2. The line integral convolution plots enabled to understand the flow physics taking place behind the results, and provided reasons for their respective evolution.

## 3.4 Comparison With literature

After having completed the AOA analysis, extra investigation was made to discover new parameters of the flow. This was done to be compared with literature, and validate or not the CFD analysis.

### 3.4.1 Set-Up

To compare the global analysis with literature, it was decided to investigate another non dimensional parameter of the flow, which is the pressure coefficient around the wing. To do so, a pressure coefficient plot was made around the wing and was compared with a plot from [12]. Even though the two airfoils aren't exactly the same, the general trend was expected to be similar.

### 3.4.2 Results and Discussion

The plot was made for the 10° rotation of the  $k - \omega$  model and is exhibited in figure 3.6, and was compared to figure 3.7 from [12].

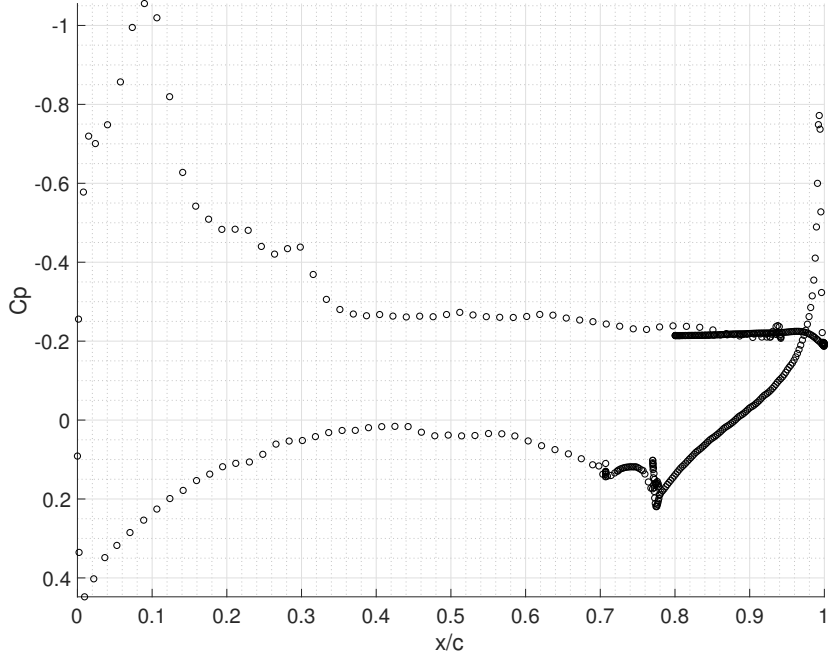


**Figure 3.6:** Pressure Coefficient Around the wing of the  $k - \omega$  model rotated by  $10^\circ$

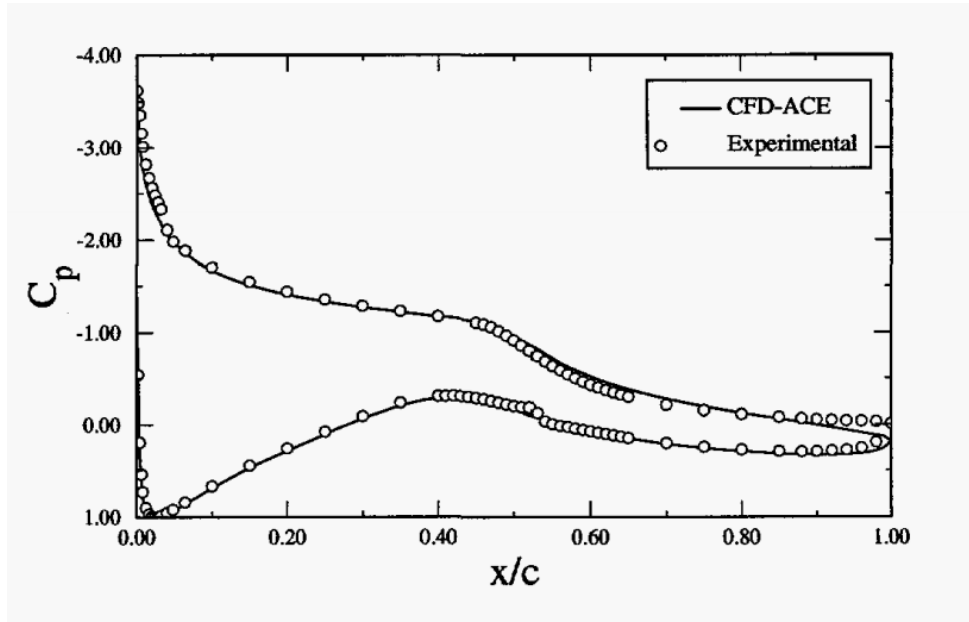


**Figure 3.7:** Pressure Coefficient Around the wing with AOA of  $10^\circ$ [12]

The general trend appears to be quite similar validating the results acknowledging the fact that the airfoils are different and cannot be compared in details. However, the very high values of pressure coefficient in the  $x/c = 1$  in figure 3.6 separate from the general trend of the values. These could suggest that the mesh at the tip of the flap might not be resolved enough. Hence, this reveals a potential flaw of the mesh design in the flap region (on the opposite side between the two engines), even though special care had been given to this region: increasing the surface size mesh and creating a specific control volume for the area.

## 4 Conclusions

The role of this was report to perform and discuss a CFD analysis of the flow around an aircraft. The analysis was performed with three different turbulence models: Standard  $k - \epsilon$ , SST  $k - \omega$ , and the Quadratic Pressure Strain Reynolds Stress model with high  $y_w^+$  wall treatment. Wall functions were used for wall treatment due to the limited computational resources. A mesh was generated using octree cells and additional prism layers, the thickness of which was set to ensure that the wall  $y_w^+$  remained in the [30, 200] range. Specific volumetric controls and surface size meshing values were defined to ensure that the mesh conserved the complex geometry of the aircraft to accurately model the flow around it. The flow physics and boundary conditions were set, and a grid refinement analysis varying the base grid size revealed that the integral quantities, namely the drag and lift coefficients varied by less than 0.03% in meshes above 1.97 million cells. The minimum takeoff speed was computed through simulations on the 1.97 million cells mesh, and was found to be approximately 2.1 times the actual literature value, slightly varying for each turbulent model. This revealed the difference between models, and the discrepancy from the actual value was assumed to be due to the poor assumptions on the mass and geometry of the aircraft at take off, as well as potential mesh design flaws. An angle of attack analysis was then held on the three different turbulent models on the 1.97 million cells mesh. The maximum lift coefficient was found to be between 5 and  $10^\circ$  for each of the three models, corresponding to stall. The trend seemed to compare adequately with literature, even though the angle seemed relatively low. Differences in the values appeared for the different models for the lift coefficient values. Vector plots of the line integral convolution of velocity were plotted to explore the physics behind the integral quantities evolution, highlighting a flow separation on the top part of the wing above stall angle of attack values. A final comparison of pressure coefficient around a cross-section of the wing was made with literature to validate the overall analysis. This report successfully reflects the impact of CFD analysis of the flow around an aircraft, revealing the potential errors which can easily be driven by incorrect meshes, and the potential it holds by reflecting crucial flow aerodynamics such as stall angle and minimum take off speeds.

## 5. References

- [1] R Murjeeb Malik. "Role of Computational Fluid Dynamics and Wind Tunnels in Aeronautics R and D". In: *Nasa Langley Research Center; Hampton, VA, United States* (Sept. 2012). URL: <https://ntrs.nasa.gov/archive/nasa/casi.ntrs.nasa.gov/20120016316.pdf>.
- [2] *C-130J-30 Super Hercules*. URL: <https://www.lockheedmartin.com/en-us/products/c130/c-130j-30-super-hercules.html>.
- [3] Pavlos Aleiferis. *ME4-CFD Individual Project: CFD analysis of the flow around an aircraft*. URL: [https://bb.imperial.ac.uk/bbcswebdav/pid-1361542-dt-content-rid-4788340\\_1/courses/DSS-ME4\\_MCFD-18\\_19/CFD\\_STAR-CCM%20\\_Aircraft\\_2018-2019.pdf](https://bb.imperial.ac.uk/bbcswebdav/pid-1361542-dt-content-rid-4788340_1/courses/DSS-ME4_MCFD-18_19/CFD_STAR-CCM%20_Aircraft_2018-2019.pdf).
- [4] *C-130 Hercules*. June 2018. URL: <https://www.af.mil/About-Us/Fact-Sheets/Display/Article/1555054/c-130-hercules/>.
- [5] Frank P. Incropera. *Principles of heat and mass transfer*. John Wiley, 2013.
- [6] W. P. Graebel. *Engineering fluid mechanics*. Taylor Francis, 2001.
- [7] Siemens. *Star CCM User Guide*. 2018.
- [8] F Menter and T Esch. "Elements of Industrial Heat Transfer Prediction". In: *16th Brazilian Congress of Mechanical Engineering* (Nov. 2001).
- [9] *Aircraft Weight and Geometry*. URL: <http://www.aerodynamics4students.com/aircraft-performance/take-off-and-landing.php>.
- [10] N. Cumpsty. *Jet Propulsion: A Simple Guide to the Aerodynamic and Thermodynamic Design and Performance of Jet Engines*. 2nd ed. Cambridge University Press, 2003. DOI: 10.1017/CBO9780511809415.
- [11] W L Sellers. "Separated flow". In: (Nov. 1986), pp. 361–374.
- [12] W.P. Wolfe and S.S. Ochs. "CFD calculations of S809 aerodynamic characteristics". In: Jan. 1997. DOI: 10.2514/6.1997-973.